Journal of Hydrology 590 (2020) 125484

Contents lists available at ScienceDirect

Journal of Hydrology

journal homepage: www.elsevier.com/locate/jhydrol

Research papers

Precipitation correction and reconstruction for streamflow simulation based on 262 rain gauges in the upper Brahmaputra of southern Tibetan Plateau

He Sun[a,b], Fengge Su[a,b,c,*]

[a] Key Laboratory of Tibetan Environment Changes and Land Surface Processes, Institute of Tibetan Plateau Research, Chinese Academy of Sciences, Beijing, China
[b] University of Chinese Academy of Sciences, Beijing, China
[c] CAS Center for Excellence in Tibetan Plateau Earth Sciences, Beijing, China

ARTICLE INFO

This manuscript was handled by Emmanouil Anagnostou, Editor-in-Chief, with the assistance of Ke Zhang, Associate Editor

Keywords:
Precipitation correction
Precipitation gradient
Hydrological modelling
Upper Brahmaputra
Tibetan Plateau

ABSTRACT

Precipitation is the key driver of terrestrial hydrological cycle and the most important atmospheric input to land surface hydrological models. However, due to high elevation, complex terrain and inaccessibility, direct meteorological observations are either sparse or nonexistent in many remote parts of Tibetan Plateau (TP), posting a great challenge in hydrological modelling studies in the TP. This is especially the case for the Upper Brahmaputra (UB) basin in southern TP. In this work, a gridded daily precipitation dataset with a spatial resolution of 10 × 10 km for 1961–2016 is reconstructed for the entire UB by combining orographic and linear corrections of China Meteorological Administration (CMA) and Global Land Data Assimilation Systems (GLDAS) data based on 262 rain gauges. The inverse evaluation of the reconstructed precipitation with a glacier-hydrology model demonstrates the accuracy and rationality of the reconstructed precipitation for hydrological modeling in the UB. The reconstructed precipitation greatly improved the precipitation estimates in the UB with the basin-averaged mean annual precipitation increased from 465 mm in the original data to 709 mm in the reconstructed data for 1961–2016. The monsoon-dominated UB basin exhibits an overall negative precipitation vertical gradient with apparent orographic effects only appearing at local scales or in small basins. Basin size and climate control should be considered when using the orographic correction approach to derive high mountain precipitation on the Tibetan Plateau. The improved precipitation estimates for the UB may best represent the real precipitation amount thus far in the UB basin and largely contribute to hydrological simulation and prediction studies in the basin.

1. Introduction

The Upper Brahmaputra (UB) (Fig. 1), also named the Yarlung Zangbo River, originates from the Gyima Yangzoin Glacier at an elevation of 5200 m in south-central Tibet and drains an area of about 253,035 km^2 (Fig. 1). It is the highest river in the world with an average elevation of greater than 4600 m. and the fifth largest river in China according to length (Guan et al., 1984). The UB is also the main fresh water source of the Tibet autonomous region and transport channels of moisture from the Indian Ocean to the inner region of the plateau (Yang et al., 1989). Like elsewhere on the Tibetan Plateau (TP), climate change has taken place in the UB (Khandu et al., 2017), with a mean annual temperature rise of 0.2–0.5 °C per decade and a mean annual precipitation increase of 3.3–8.4 mm per decade since the mid-1960s (You et al., 2007; Li et al., 2013; Yang et al., 2014; Kuang and Jiao, 2016). Along with the warming climate, a series of climate-induced changes have occurred across the UB, such as glacier retreat (Yao, 2004; Yang et al., 2011; Yao et al., 2012), snow cover decrease (Chen et al., 2018b; Li et al., 2018) and permafrost degradation (Wu and Zhang, 2010; Guo et al., 2012; Li et al., 2012; Cuo et al., 2015), which may exert substantial impacts on the hydrological cycle of the basin.

The recent changes in the UB point to the importance of understanding the interactions between climate and hydrology systems. Land surface hydrological models have been widely used to study the hydrological response to climate changes in TP river basins (Zhang et al., 2013; Lutz et al., 2014; Su et al., 2016; Tong et al., 2016; Wang et al., 2016; Kan et al., 2018). Precipitation is the key driver of the terrestrial hydrological cycle and the most important atmospheric input to land surface hydrology models, and therefore accurate precipitation inputs are essential for reliable hydrological predictions (Su et al., 2008; Ma

* Corresponding author at: Key Laboratory of Tibetan Environment Changes and Land Surface Processes, Institute of Tibetan Plateau Research, CAS, Beijing 100101, China.
E-mail address: fgsu@itpcas.ac.cn (F. Su).

https://doi.org/10.1016/j.jhydrol.2020.125484
Received 12 February 2020; Received in revised form 4 July 2020; Accepted 27 August 2020
Available online 03 September 2020

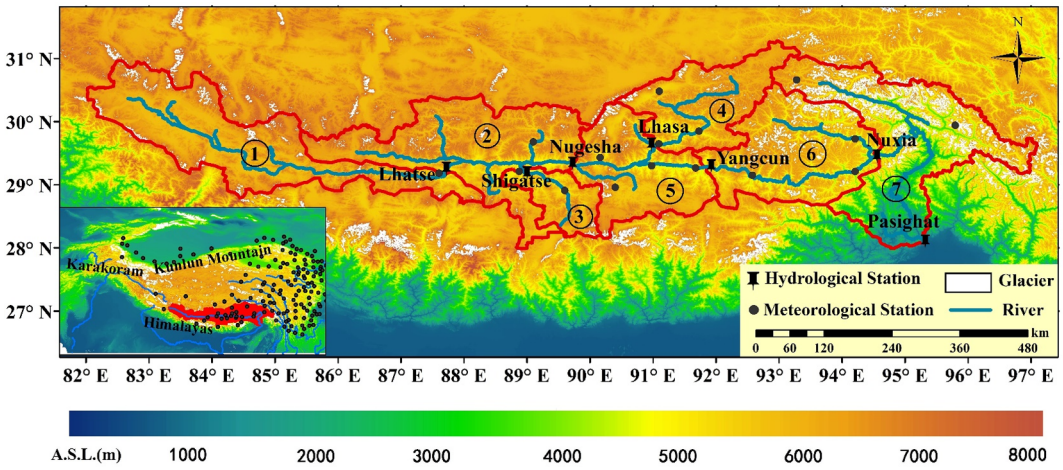

Fig. 1. Location and topography of the upper Brahmaputra (UB). The sequence numbers ①,②,③,④,⑤,⑥ and ⑦ denote the sub-basins of Lhatse (LZ), Lhatse-Nugesha (LZ-NGS), Shigatse (RKZ), Lhasa (LS), Nugesha-Yangcun (NGS-YC), Yangcun-Nuxia (YC-NX), and Nuxia-Pasighat (NX-BXK), respectively. The 16 national meteorological stations and hydrological stations are represented with black points and pushpins, respectively. Glaciers are indicated with white color.

et al., 2018). However, due to the high elevation, complex terrain and inaccessibility, direct meteorological observations are either sparse or nonexistent in many remote parts of the TP (Tong et al., 2014b; Liu et al., 2017b; Tang et al., 2018). The sparse stations are inadequate to represent the real precipitation information for the entire basin, which hampers the effective use of hydrology models in the TP (Sorooshian et al., 2011; Chen et al., 2017; Liu et al., 2017a). This is especially true in the UB basin.

A total of 16 national meteorological stations are available from the China Meteorological Administration (CMA) in the UB, most of which are located in the central and eastern valleys of the basin (Fig. 1). The gridded data obtained by interpolating observations at low altitudes tend to largely underestimate basin real precipitation due to the strong precipitation gradient created by orographic enhancements and wind-induced undercatch of solid precipitation (Immerzeel et al., 2015; Kan et al., 2018; Ma et al., 2015; Wortmann et al., 2018; Yang et al., 2005). Zhang et al. (2013) conducted flow simulations for major upstream river basins in the TP with the Variable Infiltration Capacity (VIC) hydrological model driven by gridded station data. They found a large flow underestimate in the UB compared with observed flow, due to a large underestimate in the gauge-based precipitation inputs.

Many studies have attempted to evaluate the representation of precipitation in TP basins estimated from satellite-based precipitation (Gao and Liu, 2013; Tong et al., 2014a; Ma et al., 2016; Liu et al., 2018), atmospheric reanalysis datasets (Wang and Zeng, 2012; Tong et al., 2014b; Bai et al., 2016; Chen et al., 2018a; Qi et al., 2018) and outputs of regional climate models (Maussion et al., 2014; Wortmann et al., 2018; Mimeau et al., 2019).

Satellite-based precipitation datasets provide a potential alternative source of precipitation estimates in regions where conventional in situ precipitation measurements are not readily available (Su et al., 2008; Tong et al., 2014a). Various satellite-based precipitation datasets with different temporal and spatial resolutions are available and widely used in the TP basins (Gao and Liu, 2013; Tong et al., 2014a; Liu et al., 2017a; Lu and Yong, 2018), such as the Tropical Rainfall Measuring Mission (TRMM) (Huffman et al., 2007), Global Precipitation Measurement (GPM) (Huffman et al., 2014, 2015), Climate Prediction Centre Morphing Algorithm (CMORPH) (Joyce et al., 2004), and Precipitation Estimation from Remotely Sensed Information using Artificial Neural Networks-Climate Data Record (PERSIANN-CDR) (Ashouri et al., 2015). Most of the satellite-based precipitation datasets closely agree with the monthly variations of gauge estimates, mostly due to an inclusion of gauge adjustments (Su et al., 2008; Gao and Liu, 2013; Tong et al., 2014a). Purely satellite-based estimates without including any gauge corrections tend to overestimate gauge observations (Su et al., 2011; Tong et al., 2014a) due to errors resulting from the gaps in revisit times, sampling uncertainties and retrieval algorithms (Jiang et al., 2012; Gao and Liu, 2013; Ma et al., 2016; Wang et al., 2018b).

Atmospheric reanalysis projects, based on the data assimilation system with a variety of physical and dynamical processes, produce long-term and continuous estimation of meteorological variables which have been extensively used in the TP (Wang and Zeng, 2012; Tong et al., 2014b; Qi et al., 2018; Wang et al., 2018b), such as ERA-40 (Uppala et al., 2005) and ERA-Interim (Simmons et al., 2006) developed by the European Centre for Medium-Range Weather Forecasts (ECMWF), Global Land Data Assimilation Systems (GLDAS) (Rodell et al., 2004), and Modern-Era Retrospective Analysis for Research and Application (MERRA) (Rienecker et al., 2011). However, reanalysis data tend to overestimate mean annual precipitation on the southern TP and overlook detailed regional information because of their relatively coarse grids (0.25°–2°) (You et al., 2015; Wang et al., 2017; Wortmann et al., 2018).

Another type of precipitation product comes from regional climate models that downscale global products to finer resolutions, such as the High Asia Refined analysis (HAR), which provides detailed and process-based precipitation fields at a 10-km resolution for the TP (30 km for Central Asia) for Oct 2000–Oct 2014 (Maussion et al., 2014). Several studies have suggested high potentials of the HAR data in describing high-altitude water fluxes and spatiotemporal patterns of precipitation in the TP (Maussion et al., 2014; Curio et al., 2015). However, the utility of HAR precipitation in hydrological simulations in the TP basins has not been reported.

The inherent uncertainties in current gridded precipitation products pose a great challenge to the hydrological simulation for TP basins. In addition, evaluation studies have suggested large inconsistencies among precipitation estimates from gauge observations, reanalysis data, and satellite retrievals in the UB (Table 1) (Zhang et al., 2013; Tong et al., 2014b; Huang et al., 2016; Qi et al., 2018), leaving actual areal precipitation information in the UB still unknown.

A few attempts have been made to derive high mountain precipitation estimates through different approaches for the TP basins, including: (1) inversed modeling approach based on glacier mass balance (Immerzeel et al., 2015; Wortmann et al., 2018); (2) multiple precipitation datasets merging method (He and Yang, 2011; Chen et al., 2017; Ma et al., 2018; Qi et al., 2018); (3) linear corrections based on two time series of precipitation and/or streamflow (Zhang et al., 2013; Zhou et al., 2014); and (4) orographic corrections (Dahri et al., 2016; Kan et al., 2018; Wang et al., 2018a).

Table 1
Summary of relevant studies on precipitation in the NX or entire UB basins.

Relevant studies	Mean annual precipitation (mm)	Study area	Period	Data	Data source
Nie et al. (2012)	468.8	UB	1978–2009	27 CMA Station Data	IDW Interpolation
Zhang et al. (2013)	540	NX	1961–1999	Corrected CMA	Correction by Linear Relationship between Annual Precipitation and Simulated Runoff
Yang et al. (2014)	428.7	UB	1961–2010	6 CMA Station Data	CMA Interpolation
Li et al. (2015)	512.4	UB	1961–2014	16 CMA Station Data	Thin Plate Spline Interpolation
Bai et al. (2016)	478	NX	1979–2010	Monthly Grid-based Precipitation Data with a 0.5° Resolution from CMA	CMA Interpolation
Huang et al. (2016)	300–500	UB	1973–2013	CMA and GLDAS	IDW Interpolation
Tong et al. (2014b)	462.8	NX	1998–2009	TMPA	
	360.4		1961–2007	APHRODITE	
	897.5		1961–1990	UW Precipitation Data	
	897.6		1961–2001	ERA-40	
	1236.6		1979–2009	ERA-Interim	

Note: CMA = China Meteorological Administration; TMPA = TRMM Multi-satellite Precipitation Analysis; UW = University of Washington; IDW = Inverse Distance Weighting; APHRODITE = Asian Precipitation- Highly-Resolved Observational Data Integration Towards Evaluation of the Water Resources; ERA = reanalysis data set produced by the European Center for Medium-Range Weather Forecasts.

Given the large area of the UB basin (253,035 km^2), sparse stations, and complex terrain precipitation mechanisms, a single correction approach may not fit the entire basin. Fortunately, a field research campaign has been carried out since 2017, with 12 rain gauges and 12 temperature sensors at different altitudes, installed under the Second Tibetan Plateau Scientific Expedition and Research (STEP) project let by the Institute of Tibetan Plateau Research, Chinese Academy of Sciences (http://data.tpdc.ac.cn). In addition, monthly precipitation data from more than 200 rain gauges within the UB for 2014–2016 were collected from the Tibet Autonomous Region Hydrology Bureau (TARHB). The newly installed and established rain gauges together with existing national meteorological stations, with elevations ranging between 1500 m and 5300 m, constitute a unique observation basis to derive reliable precipitation estimates in the UB basin.

In this work, our intent is to reconstruct a reliable precipitation dataset for streamflow simulation in the entire UB by combining orographic and linear correction approaches based on 262 gauge observations. The reconstructed precipitation is used to drive the VIC hydrological model linked with a temperature-index model (VIC-Glacier) (Zhang et al., 2013; Su et al., 2016; Tong et al., 2016; Kan et al., 2018; Meng et al., 2019), and is inversely evaluated by comparing with observed discharge, glacier area changes, and MODIS-based snow cover faction (SCF) data in the UB. The reconstructed precipitation is also compared with widely used estimates from different data sources in the UB basin. The specific goal of this work is to provide reliable and accurate precipitation estimates for hydrological modeling and projection studies in the UB, and to provide a reference for deriving high mountain precipitation in the TP with complex terrain and climate controls and limited observations.

2. Data and method

In this work, the precipitation correction and reconstruction are at the sub-basin basis. The entire UB is divided into seven sub-basins from upstream to downstream on branches or river stems (Fig. 1; Table 2). They are the upstream basins of Lhatse (LZ), Shigatse (RKZ) and Lhasa (LS), the regions between Lhatse and Nugesha (LZ-NGS), between Nugesha and Yangcun (NGS-YC), between Yangcun and Nuxia (YC-NX) and the regions between Nuxia and Pasighat (NX-BXK). Among the sub-basins, the YC-NX has the largest runoff contribution (~51%) to total flows at the Nuxia hydrological station (Fig. 1; Table 2), followed by the LS, LZ-NGS, LZ, NGS-YC and RKZ sub-basins with contributions of 3–16% to total flows at the Nuxia. Glacier coverages range from 0.27% to 9.84%, with the largest distributed in the downstream sub-basins of YC-NX and NX-BXK. The mean snow cover fraction (SCF) ranges between 7% and 32% among the sub-basins with a mean SCF of 19% over the entire UB (Table 2).

2.1. Precipitation data

The data used for the precipitation reconstruction in the UB include daily precipitation data from 16 meteorological stations of CMA (Fig. 1) for 1961–2016, monthly precipitation data from 262 rain gauges for 2014–2016 and the daily atmospheric reanalysis precipitation dataset (GLDAS) for 1961–2016 (Table 3).

Gauge-based CMA data Most of the CMA stations (Fig. 1) are located in the downstream low valleys, with elevations of 2700–4500 m (70% of the UB is at elevations higher than 4500 m). The number of stations within each sub-basin is listed in Table 3, with the most (3–4 stations) lying in the upstream basins of LS, NGS-YC and YC-NX and the least in the upstream basins of LZ and LZ-NGS (0–2 stations). These CMA station data are used as a basis for precipitation corrections, which are interpolated to 10 km × 10 km grids by the inverse distance weighting (IDW) method.

Rain gauge data Monthly precipitation data from 262 rain gauges with elevations of 1500–5200 m are collected from the TARHB for 2014–2016 (Table 3). The number of stations within each sub-basin ranges between 16 and 77 (Table 3), with the YC-NX has the most (77) followed by the LS (51). In spite of the short time span (three years) of these data, the relatively dense station coverage within each sub-basin allows a linear correction for the gridded CMA data at annual scales (See Section 3.2).

GLDAS precipitation data The GLDAS is an atmospheric reanalysis precipitation dataset, which uses advanced land surface modeling and data assimilation techniques to generate optimal fields of land surface states and fluxes (Rodell et al., 2004). The 0.25°×0.25° 3-hourly GLDAS-2 precipitation data is obtained from https://hydro1.gesdisc.eosdis.nasa.gov/data/GLDAS/GLDAS_NOAH025_3H.2.0/doc/README_GLDAS2.pdf. The GLDAS_NOAH025_3H_2.0 precipitation data for 1961–2010 and the GLDAS_NOAH025_3H_2.1 for 2011–2016 are used as a basis for precipitation corrections for the LZ sub-basin (See Section 3.2).

The mean annual precipitation of several widely used precipitation datasets are used to compare with reconstructed data in the UB basins, including the gauge-based APHRODITE (Yatagai et al., 2012), satellite-based PERSIANN-CDR (Ashouri et al., 2015) and GPM (Huffman et al.,

Table 2
Characteristics of seven sub-basins in the UB.

		LZ	LZ-NGS	RKZ	LS	NGS-YC	YC-NX	NX-BXK
Hydrological station		Lhatse	Nugesha	Shigatse	Lhasa	Yangcun	Nuxia	Pasighat
Location	Latitude (°)	29.05	29.32	29.25	29.63	29.28	29.47	28.1
	Longitude (°)	87.38	89.71	88.88	91.15	91.88	94.57	95.53
Drainage area (km^2)		50,553	45,327	11,064	26,235	26,599	41,770	51,507
Basin average elevation (m)		5370	4983	5353	5272	4767	4937	3711
Period of streamflow		1980–2000	1980–2000	1980–2000	1980–2000	1980–2000	1980–2000	–
Discharge (m^3/s)		172.18	202.15	55.16	300.02	163.87	920.31	–
Contribution to the total runoff (%) at the Nuxia station		9.17	11.09	3.76	15.98	8.99	51.01	–
Glacier coverage (%) *		1.49	0.27	1.11	0.89	1.64	2.52	9.84
Snow cover fraction (%) ** (2001–2014)		15.58	7.12	6.98	23.08	10.21	24.25	31.97

*Glacier data is from the Tibetan Plateau Glacier Datasets in 2013 (Ye et al., 2017), http://www.tpedatabase.cn.
**Snow cover fraction is from the Moderate Resolution Imaging Spectroradiometer (MODIS)10C2, https://nsidc.org/data.

2014, 2015), reanalysis data of ERA-Interim (Simmons et al., 2006), and the outputs of the regional climate model HAR (Maussion et al., 2014). The information of those precipitation products can be found in Supporting information Table S1. To facilitate direct comparisons between reconstructed data and those widely used precipitation datasets, all the gridded data set were regridded to 10 × 10 km grids using the nearest neighbour method.

2.2. Approaches of precipitation correction and reconstruction

In this work, the precipitation reconstruction for the UB is conducted by combing the orographic and linear correction approaches.

2.2.1. Orographic correction

Here, we first analyze the relationship between mean annual precipitation estimates with the 262 rain gauges in 2014–2016 (Table 3) and elevation over the seven sub-basins (Fig. 1, Table 2). If a significant positive relationship is observed in a certain basin, the orographic correction is applied when the CMA station data is interpolated from low elevations to 10 × 10 km grids in the basin:

For grid i and year *s*,

$$P_i^{'}=(P_i + P_i/P_{annual}^{s} \times (Ele_{grid} - Ele_i) \times PG (i = 1, 2, \cdots, n)$$

where $P_i^{'}$ is corrected daily precipitation (mm) of grid *i*; P_i is original CMA interpolated daily precipitation (mm) of grid *i*; $P_{annual}^{s}$is CMA interpolated annual precipitation of grid *i* in year *s*; $Ele_{grid}$is mean elevation (m) of grid *i*; $Ele_i$is the elevation (m) of rain gauge; *PG* is the precipitation gradient; and *n* is the number of rain gauges.

2.2.2. Linear correction

Linear correction is applied to the basins where orographic lifting effects are not observed and at least one CMA station is within the basin (Table 3). In this approach, linear regressions are performed between mean annual precipitation from the interpolated CMA data at 10 km × 10 km grids and the TARHB gauges fall into the same grids for each sub-basin. Where there are at least two gauges in the pixel of gridded product, we used the average value of the gauges to correct the corresponding gridded precipitation data. A linear relationship is thus developed based on the regression results in the basin: y = a × x + b, where y is annual corrected precipitation; x is annual CMA gridded data.

For the LZ sub-basin (Fig. 1) where there are no CMA stations (Table 3), the gridded GLDAS precipitation data is used in the LZ to compare with the TARHB gauge data because of its long-term series (1961–present).

2.3. Hydrological model

The VIC model (Liang et al., 1994, 1996) is a semi-distributed macroscale land surface hydrological model, which parameterizes the dominant hydrometeorological processes taking place at the land surface-atmosphere interface. The model solves both surface water and energy balance within the grid cell. In this study, the VIC linked with a simple degree-day glacier melt algorithm (Hock, 2003), called the VIC-Glacier model, is used to evaluate the accuracy of the reconstructed precipitation in the UB. The VIC-Glacier model has been previously used in flow simulations for major river basins in the TP (Zhang et al., 2013; Su et al., 2016; Tong et al., 2016; Kan et al., 2018; Meng et al., 2019). Here, the modeling framework at a three-hourly time step and

Table 3
Information of rain gauge observations for the UB basins.

		LZ	LZ-NGS	RKZ	LS	NGS-YC	YC-NX	NX-BXK	UB
National meteorological stations from the CMA (1961–2016)	Number		2	2	3	4	3	2	16
	Elevation (m)		4000	3800–4100	3000–4200	3500–4400	2900–3300	2700–4500	2700–4500
	Longitude (°E)		87.38–89.09	88.96–89.59	90.93–91.75	90.12–91.77	92.56–94.48	93.26–95.91	87.38–95.91
	Latitude (°N)		29.05–29.68	28.91–29.18	29.61–30.49	28.93–29.45	29.13–29.58	29.98–30.65	29.05–30.65
Rain gauges from the TARHB (2014–2016)	Number	16	25	32	51	39	77	22	262
	Elevation (m)	3900–5200	3800–5000	3800–4600	3600–4800	3500–4700	2800–4800	1500–5000	1500–5200
	Longitude (°E)	84.76–88.16	86.94–89.52	88.58–89.74	90.93–92.33	89.72–91.50	91.95–94.46	93.17–96.29	84.76–93.17
	Latitude (°N)	28.80–29.81	28.84–29.75	28.45–29.25	29.63–30.68	28.98–30.04	28.68–30.35	29.49–30.71	28.80–30.71
Rain gauges from the STEP (2017–2018)	Number	4		2	2		4		12
	Elevation (m)	4300–5300		4400–4500	4300–4800		3200–4500		3200–5300
	Longitude (°E)	82.44–87.23		89.35–89.61	92.05–92.57		92.33–93.66		82.44–93.66
	Latitude (°N)	29.30–30.60		28.18–28.45	30.43–30.96		29.71–29.88		29.30–30.96

Note: CMA = China Meteorological Administration; TARHB = Tibet Autonomous Region Hydrology Bureau; STEP = Second Tibetan Plateau Scientific Expedition and Research Project.

1/12° × 1/12° (around 10 km × 10 km) spatial resolution in the UB was adopted from Zhang et al. (2013). The required climate forcing data in the VIC model include daily precipitation, maximum and minimum temperature and wind speed. The temperature data from the 16 CMA stations are adjusted by lapse rates of −0.80 °C/100 m in January–March, −0.70 °C/100 m in April–May, −0.56 °C/100 m in June, −0.40 °C/100 m in July–September, and 0.58 °C/100 m in October–December in the gridding process. The land surface characteristic files of soil texture, topography, and vegetation types are from Zhang et al. (2013).

Observed streamflow, glacier area changes, and satellite-based snow cover extent data are used to calibrate and validate the VIC-Glacier model driven by the reconstructed precipitation. Monthly observed streamflow data at the Lhatse, Shigatse, Nugesha, Lhasa, Yangcun and Nuxia hydrological gauge stations on the tributaries and main stream of UB for 1980–2000 are from the Qinghai and Tibetan hydrological bureaus. The Moderate Resolution Imaging Spectroradiometer (MODIS) 10C2 reporting the maximum percentage of snow cover during an 8-day period in 0.05° resolution grid (Hall et al., 2002) (https://nsidc.org/data) is used to calculate the snow cover fraction (SCF) and to compare with VIC-Glacier model simulations in the UB.

Glacier data in the first Chinese Spatial Glacier Inventory from the "Environment & Ecological Science Data Center for west China" (http://westdc.westgis.ac.cn/glacier) is used to provide the initial glacier distribution in the VIC-Glacier model. Ye et al. (2017) generated glacier area coverages on the Tibetan Plateau based on Landsat satellite images from three epochs: 263 in the mid-1970s, 150 in 1999–2002, and 148 in 2013–14. The most frequent year in each period was defined as the reference year for the three mosaics (M1976, M2001 and M2013) (Ye2017 hereafter). The volume-area scaling approach (Bahr et al., 1997) is used to update the calculated glacier area and volume in the VIC-Glacier model every year.

Two categories of model parameters are needed to calibrate in the VIC-Glacier model: (1) The degree day factors (DDFs) of both snow (DDF_snow) and glaciers (DDF_glacier) for simulating the meltwater in glacierized areas; and (2) the parameters of the VIC model for simulating runoff process in nonglacierized areas.

The initial values of DDF_glaciers are derived from previous studies based on observed glacier mass balance data in the sub-basins of UB, and are then further adjusted to match the observed glacier area changes in 1970–2016. The DDF_glacier for the LZ, LZ-NGS and RKZ sub-basins is set to 10.97 $mm^{\circ}C^{-1}$ day^{-1} based on Yala Glacier (Kayastha, 2001); 9.2 $mm^{\circ}C^{-1}$ day^{-1} in the LS and NGS-YC based on Zhadang Glacier (Wu et al., 2010); and 6.2 $mm^{\circ}C^{-1}$ day^{-1} in the YC-NX and NX-BXK based on Yanlongba Glacier (Liu and Zhang, 2018). The DDF_snow is set to 5.3–5.6 $mm^{\circ}C^{-1}$ day^{-1} among the sub-basins based on the relationship between DDF_glacier and DDF_snow (Singh et al., 2000; Zhang et al., 2006; Kumar et al., 2016).

In the VIC model, the first and second soil layers depth (D1, D2) and the infiltration parameter (B_inf) have been identified as the most sensitive parameters (Su et al., 2005; Zhang et al., 2013). The B_inf which defines the shape of the Variable infiltration capacity curve has a common range of 0–0.4. A top thin soil layer depth (D1) of 0.05–0.10 cm is usually used, as suggested Liang et al. (1996) to improve evapotranspiration simulation in arid climates. Previous studies have suggested a much larger sensitivity of D2 than the other two parameters (Zhang et al., 2013). In this work, the topsoil layer depth (D1) for each grid cell is set to 0.1 m, and the B_inf is set to 0.2 without further calibration. The second soil layer depth D2 mainly determines the moisture storage capacity in the model. The D2 is usually calibrated at basin scales to match observed streamflow, and therefore, is highly dependent on the precipitation input. Driven by the reconstructed precipitation and carefully determined parameters of DDFs, the final values of D2 are 0.8–1.3 m among the sub-basins. The correlation coefficient (R), Nash-Sutcliffe efficiency (NSE) and relative error (Bias, %) are used to evaluate the agreement between the VIC-Glacier model simulations and observations.

3. Correction and reconstruction of precipitation in the UB

3.1. Orographic correction of precipitation in the RKZ sub-basin

Fig. 2 shows scatter plots of mean annual precipitation (2014–2016) from the 262 TARHB gauges against elevation in the seven sub-basins and the entire UB. The sub-basins of LZ, LZ-NGS and NGS-YC with drainage areas of 26,000–51,000 km^2 (Table 2) are located in the main stream of the UB (Fig. 1). These three basins show weak decreasing tendencies of annual precipitation with elevation, as reflected by a very low negative slope of −2 to −7 mm/100 m (Fig. 2a, b, e). However, local signals of orographic lifting are observed in certain elevation bands in these basins. For example, mean annual precipitation significantly increases with elevation at 9.2 mm/100 m (R of 0.62) at the altitudes of 4200–4500 m in the LZ, 17.2 mm/100 m (R of 0.87, $p < 0.1$) at 4500–4900 m in the LZ-NGS and 11.2 mm/100 m (R of 0.62, $p < 0.1$) at 4200–4700 m in the NGS-YC sub-basin.

The YC-NX, also lying in the main stream of UB with a drainage area of 41,770 km^2 (Fig. 1, Table 2), displays two contrasting patterns of precipitation gradient (Fig. 2f). One group, consisting of 30 rain gauges and lying on the north of YC-NX, exhibits a significantly decreasing trend with elevation (-13 mm/100 m, R of 0.69, $p < 0.01$), while another group, consisting of 47 rain gauges and lying on the south of YC-NX, shows a significantly increasing trend of annual precipitation with elevation (5 mm/100 m, R of 0.55, $p < 0.01$).

The RKZ and LS are two independent branches of the UB, with RKZ in the south of UB and LS in the north (Fig. 1). The southern tributary RKZ, with an area of 11,064 km^2, shows a strong increasing trend of annual precipitation (13 mm/100 m, R of 0.75, $P < 0.01$) with elevation (Fig. 2c), similar to the change pattern of the southern YC-NX (Fig. 2f). However, the northern basin LS, with an area of 26,235 km^2, presents a general weak decreasing trend (-3 mm/100 m, R of 0.37) of precipitation (Fig. 2d), mimicking the change tendency of northern YC-NX sub-basin (Fig. 2f).

The NX-BXK sub-basin lies in the very downstream of the UB (Fig. 1), with mean annual precipitation of 600–2000 mm based on 22 TARHB gauges in 2014–2016. Basin precipitation displays a statistically significant decrease with elevation (−28 mm/100 m, R of 0.64, $P < 0.01$) (Fig. 2g).

For the entire UB, two groups of rain gauges with distinct change patterns are also identified (Fig. 2h). One group with mean annual precipitation of more than 700 mm, mostly from the rain gauges in the NX-BXK and northern YC-NX, shows a significantly decreasing trend of precipitation (−28 mm/100 m, R of 0.75, $p < 0.01$). While another group with mean annual precipitation < 700 mm, mainly from the rain gauges in the southern YC-NX and its upstream sub-basins, exhibits a slightly decreasing trend of precipitation with elevation (−4 mm/100 m, R of 0.22).

In summary, mean annual precipitation generally shows decreasing trends with elevation in all the basins except for the RKZ (Fig. 2c), while local signals of orographic lifting exist in certain elevation bands in the UB basins. Precipitation in the UB is mostly affected by the prevailing atmospheric circulation combined with the effects of local elevation and terrain (Liu et al., 2007; Zhang et al., 2016). The overall negative precipitation vertical gradient in the UB may be associated with a decreasing trend of large-scale water vapor transport from the Indian Ocean with the increased elevation that overwhelms the terrain effects (Sun et al., 2020). Hence, the orographic correction with a gradient of

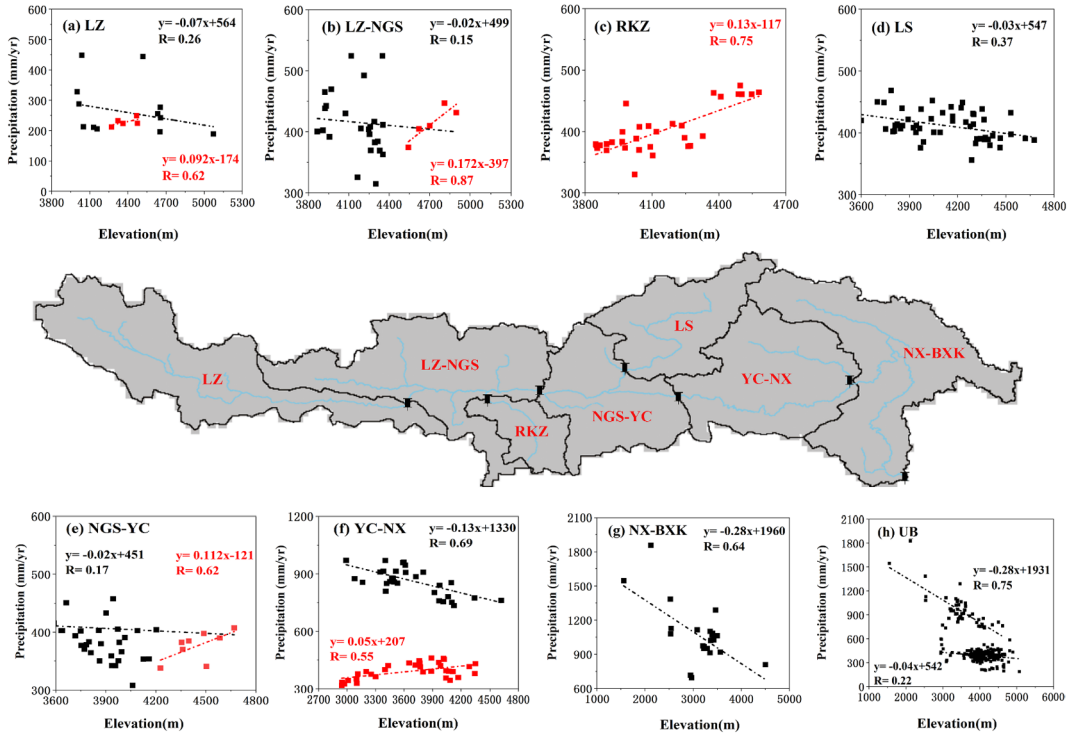

Fig. 2. Scatterplots of mean annual precipitation from rain gauges against elevation for 2014–2016 in the UB and its sub-basins.

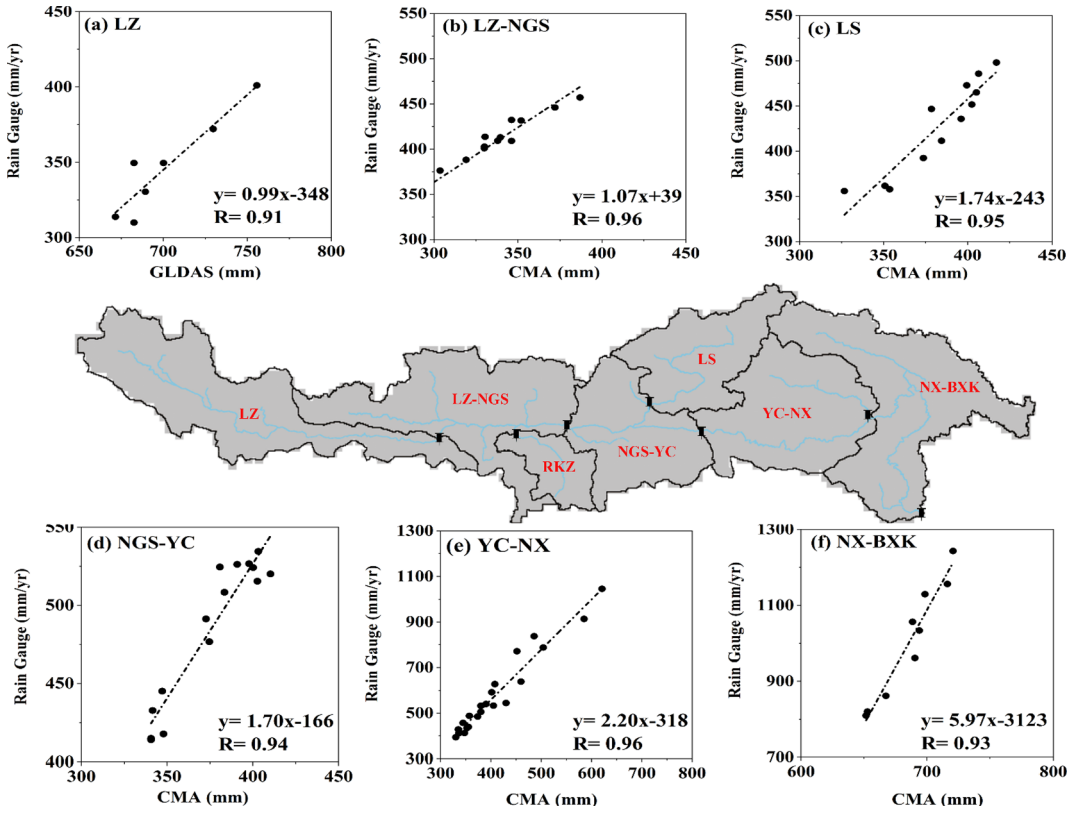

Fig. 3. Scatterplots between mean annual precipitation from rain gauges and the corresponding CMA gridded data (GLDAS for the LZ) in six sub-basins of the UB for 2014–2016.

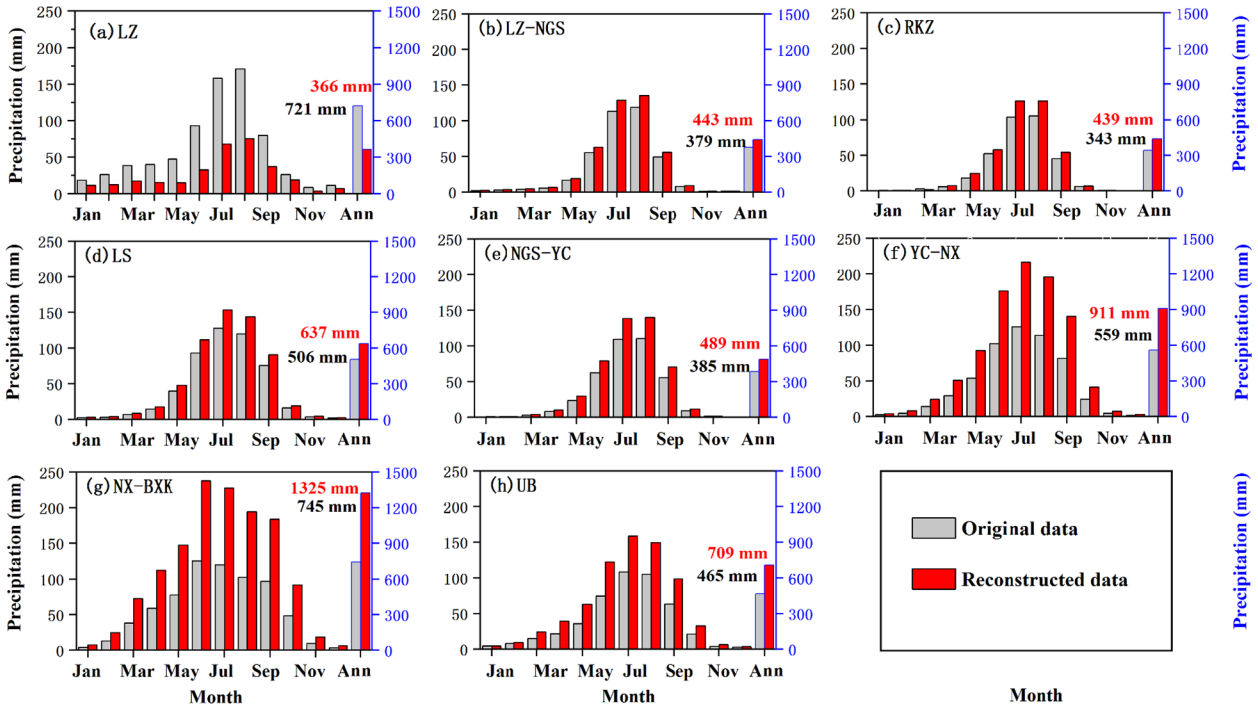

Fig. 4. Seasonal cycle and mean annual precipitation estimate from the gridded CMA and reconstructed precipitation data in the seven sub-basins and entire UB for 1961–2016.

13 mm/100 m is only applied in the RKZ sub-basin where precipitation presents significant vertical gradients (Fig. 2c).

3.2. Linear correction of precipitation

Fig. 3 shows the scatterplots of mean annual precipitation from the TARHB gauges against the corresponding CMA gridded data for 2014–2016 in all the sub-basins except for the RKZ. For the LZ, the GLDAS gridded precipitation data is used to compare with the TARHB gauge data.

There is generally good correspondence between the TARHB gauges and CMA grids with R of 0.91–0.96 ($p < 0.01$) among the basins (Fig. 3). However, the gridded CMA precipitation data tend to underestimate the TARHB gauge estimates in the LZ-NGS, LS, NGS-YC, YC-NX, and NX-BXK by 10–32% (Fig. 3b–f). The underestimates increase from upstream to downstream with the largest underestimation occurring in the very downstream YC-NX and NX-BXK (30–32%). On the other hand, the GLDAS gridded data tend to overestimate the TARHB gauges by more than 100% in the LZ (Fig. 3a).

The linear regression equations derived from the scatterplots ($y = 0.99x - 348$ for LZ, $y = 1.07x + 39$ for LZ-NGS, $y = 1.74x - 243$ for LS, $y = 1.70x - 166$ for NGS-YC, $y = 2.20x$-318 for YC-NX and $y = 5.97x - 3123$ for NX-BXK) are thus used to correct the CMA/GLDAS gridded data in the corresponding basins (Fig. 3a–f). Together with the orographic correction of CMA data in the RKZ, a daily gridded precipitation dataset at 10 km × 10 km grids is reconstructed covering the entire UB for 1961–2016.

Fig. 4 shows seasonal cycle and mean annual precipitation estimates from the reconstructed precipitation and the original gridded CMA data (GLDAS for the LZ) in the seven sub-basins and the entire UB for 1961–2016. Overall, the corrections greatly increase the precipitation estimates in the UB from a mean annual precipitation of 465 mm in the original estimates to 709 mm in the reconstructed data, which is also much larger than the previous gauge-based estimates in the UB (428–469 mm, Table 1). Regarding the sub-basins, the corrections reduced about 50% of the original GLDAS estimates in the LZ, resulting in mean annual precipitation of 366 mm after the linear correction (Fig. 4a). In the other basins, the corrections generally increase the original CMA gridded estimates by 17–78% among the basins, resulting in a mean annual precipitation of 439–1325 mm from upstream to downstream UB. All the sub-basins show similar precipitation regimes with 70–90% of annual totals occurring in June–September and 10–30% in the other months, reflecting the dominant effects of monsoon systems and occasional intrusions of westerlies.

4. Hydrological evaluation of the reconstructed precipitation

The reliability of hydrological simulations is highly dependent on the accuracy of precipitation input. Hydrological models have been adopted as a useful tool in verifying catchment-wide precipitation estimates by calibrating them to available hydrological observations (Duethmann et al., 2013; Immerzeel et al., 2015; Wortmann et al., 2018). In this section, the VIC-Glacier model is driven by the daily reconstructed precipitation, and the model simulations are compared with observed streamflow, glacier area changes and snow cover extent to inversely evaluate the rationality of the reconstructed precipitation in the UB.

4.1. Streamflow simulation

Precipitation plays a dominant role in runoff generation in the UB, with a high correlation between the annual variation of precipitation and streamflow (R of 0.74, $p < 0.01$) during 1961–1999 (Zhang et al., 2013). Therefore, the accuracy of simulated streamflow can reflect the rationality of precipitation input to a large extent in the monsoon dominated UB basin.

Fig. 5 shows the VIC-Glacier simulated mean monthly streamflow of each sub-basin (Fig. 5a–f) and the entire region upstream of the Nuxia

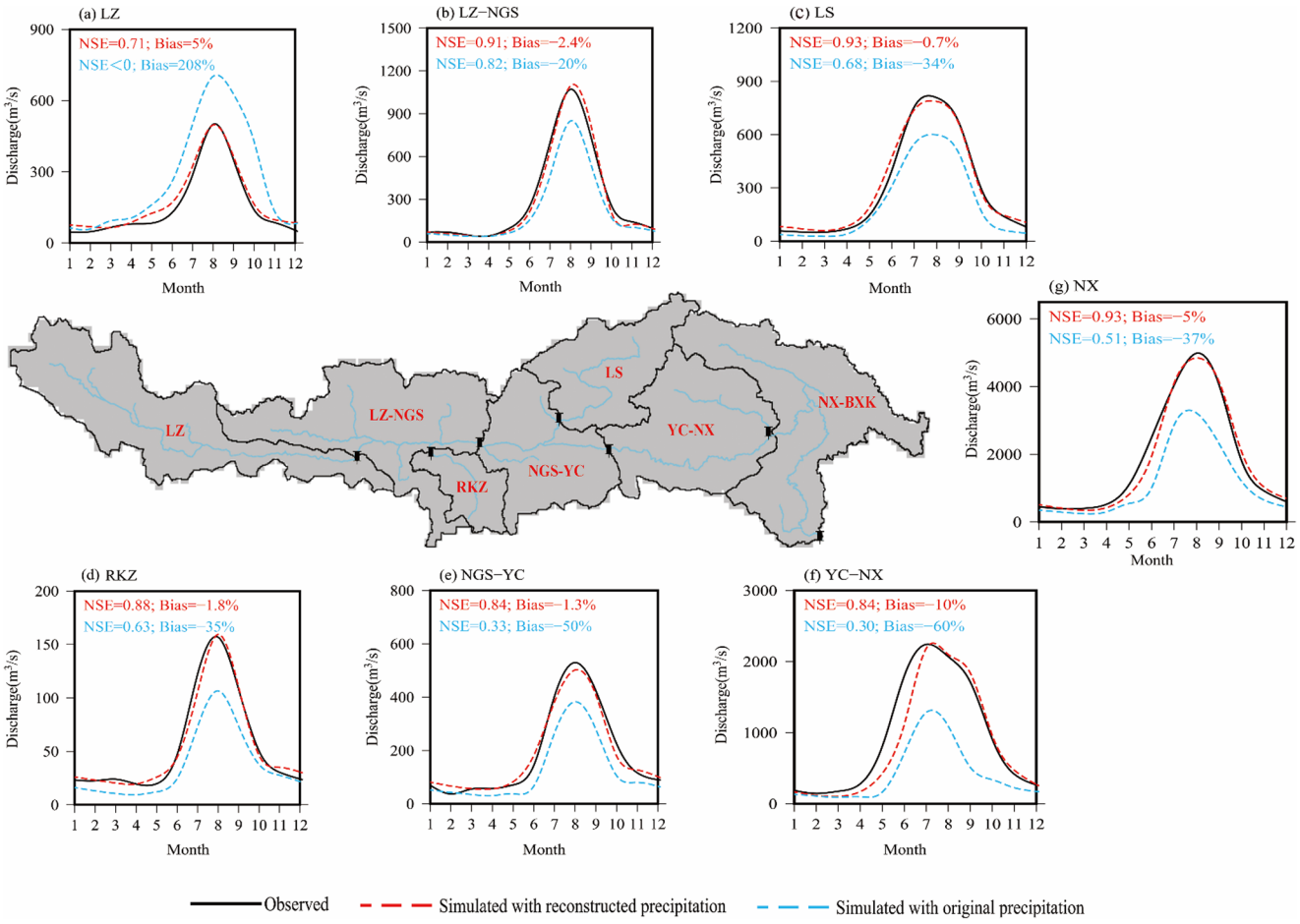

Fig. 5. Mean monthly streamflow simulated with the reconstructed precipitation and original gridded data in the six sub-basins and the entire domain (NX) for 1980–2000.

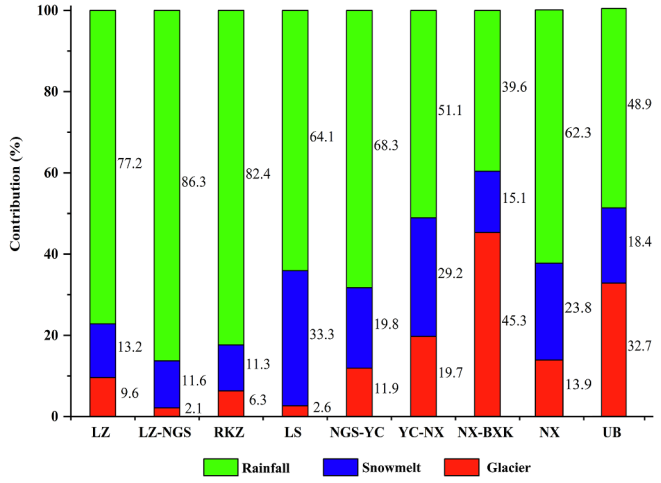

Fig. 6. Contributions of rainfall, snowmelt, and glacier runoff to the total annual runoff for the seven sub-basins and entire UB basins for 1980–2000.

station (NX, Fig. 5g), forced by the reconstructed precipitation for 1980–2000. For the purpose of comparison, the model results forced by the original precipitation data are also included. The reconstructed precipitation-driven model results can successfully reproduce both monthly (Fig. S1) and seasonal patterns (Fig. 5) of observed streamflow in the UB basins, with NSE of 0.7–0.9 and bias of mostly within ± 5%. The flow simulations are significantly improved when compared with those forced by the original data, where there is a positive bias of 208% in the LZ (Fig. 5a) and negative bias of 20–60% in other basins (Fig. 5b–f).

Fig. 6 shows the contributions of rainfall, snowmelt and glacier runoff to the total annual flow of each sub-basin and the entire domain of the UB for 1980–2000 based on the model results forced by the reconstructed precipitation. The rainfall runoff contribution ranges from 40% to 86% among the sub-basins, with an average of about 49% for the entire UB, suggesting a dominant water source of rainfall runoff in the UB. The contribution of snowmelt is about 11–33% among the sub-basins, with an average of about 18% for the entire UB. Relatively larger snowmelt contributions (15–33%) are presented for the downstream basins of LS, NGS-YC, YC-NX and NX-BXK. Glacier runoff contributions range from 2% to 45% among the sub-basins, with the least in the LZ-NGS and the most in the NX-BXK, consistent with the glacier coverage within each basin (Table 2). On average, about 33% of annual total runoff comes from glacier runoff in the entire UB.

4.2. Glacier area change

Remotely sensed glacier coverage data offer a valuable alternative to ground observation in the evaluation of glacier-hydrological models. Here the glacier area coverage (%) in the UB basins in 1976, 2001 and

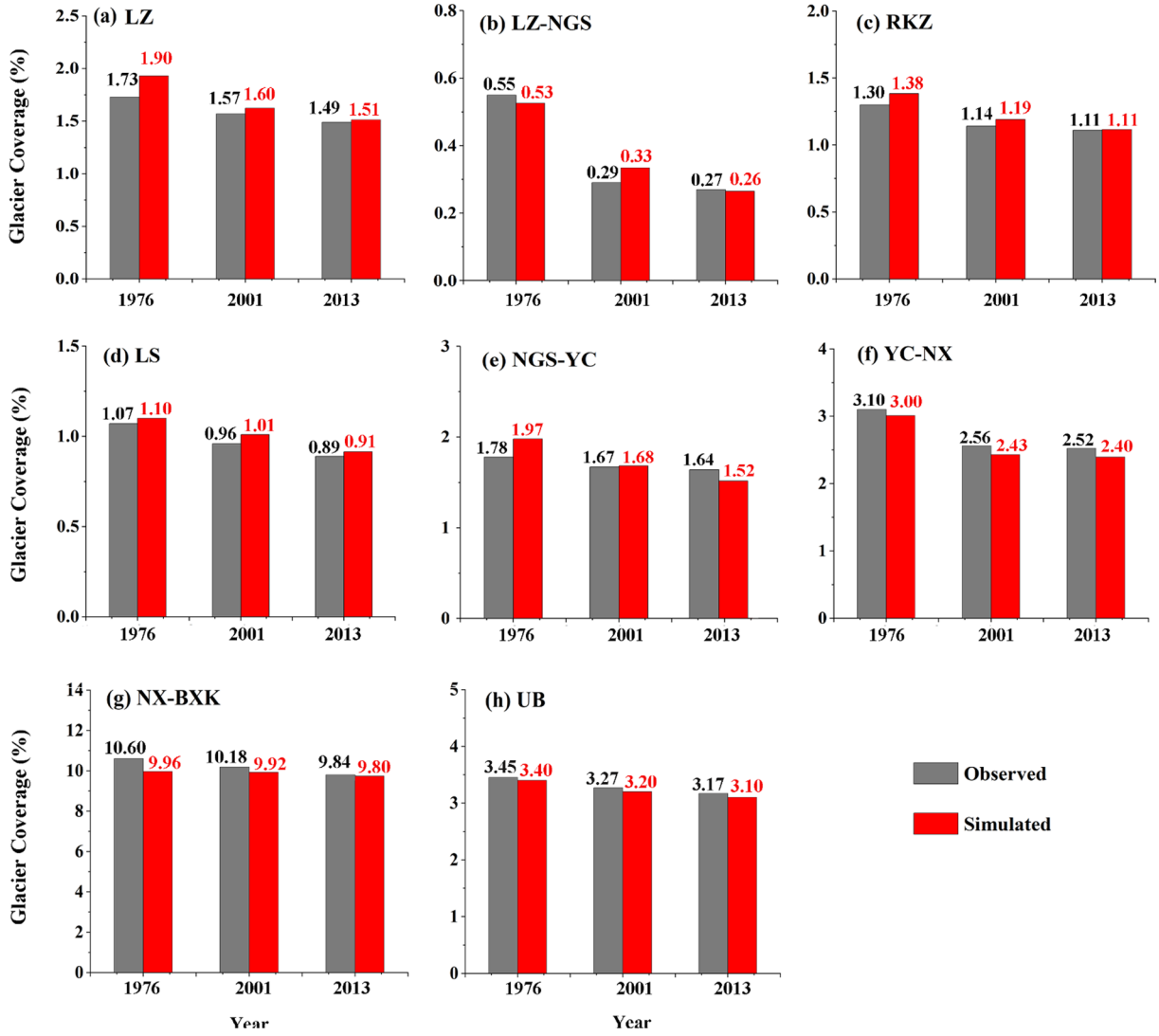

Fig. 7. Glacier coverage (%) from the VIC-Glacier model simulation and satellite-based observation in the seven sub-basins and entire UB in 1976, 2001, and 2013, respectively.

2013 derived from Landsat satellite images in Ye et al. (2017) is used to compare with the VIC-Glacier model simulated glacier areas (Fig. 7).

In the data of Ye2017, the glacier area generally shows a decreasing trend in the UB basins from 1976 to 2013, with glacier area reductions of 4–47% in 2001 and 7–51% in 2013 relative to 1976 data, resulting in a mean glacier area shrinkage of 5% and 8% in the UB in 2001 and 2013, respectively (Table S2). The largest glacier shrinkage tends to occur in the basins with the least glacier coverage (e.g., LZ-NGS), while the least shrinkage is observed in the basins with the largest glacier coverage (e.g., NX-BXK) (Table S2). The VIC-Glacier simulated glacier areas exhibited a close agreement with the Ye2017 in 1976, 2001, and 2013 with relative bias mostly < 10% in the basins (Fig. 7, Table S2). The VIC-Glacier model also simulated a decreasing trend of glacier area, with glacier area reductions of 5–40% in 2001 and 7–53% in 2013 relative to the 1976 data among the basins (Table S2). The good agreement between the two completely independent estimates from the Ye 2017 data and VIC-Glacier model partly confirms the rationality of the reconstructed precipitation as the model input.

4.3. Snow cover fraction

There is a large spatial heterogeneity of snow cover in the UB, with mean annual snow cover fraction (SCF) ranging from 7% to 32% among the sub-basins in terms of the MODIS data, with the heaviest snow concentrated in the very downstream basins (Table 2). The sub-basins of LZ, LS, YC-NX and NX-BXK, which account for about 95% of total MODIS-estimated snow-covered area in the UB (Table 2), were chosen to evaluate the VIC-Glacier model SCF simulations (Fig. 8).

Fig. 8 shows the annual cycle of MODIS and VIC-Glacier model simulated SCF (%) forced by the reconstructed precipitation in the LZ, LS, YC-NX and NX-BXK for 2001–2014. For the purpose of comparison, the model results forced by the original precipitation data are also included. There is a strong seasonal variation in the MODIS SCF with the highest appearing in October–March (15–55%) and lowest in June–August (< 6–8%) in the selected basins (Fig. 8). Both the model simulated SCF forced by the reconstructed and original precipitation can follow the seasonal variation of the MODIS with R of 0.77–0.97 ($p < 0.01$, Fig. 8) in the four basins. However, the simulated SCF forced by the reconstructed precipitation tends to underestimate the MODIS with a mean negative bias of 17–43%, with the largest underestimate in the YC-NX and the least in the LZ. The underestimates mostly appear in summer in the LZ, and in spring and winter seasons in the other three basins (Fig. 8). On the other hand, the simulated SCF forced by the original precipitation exhibits even larger biases, with a positive bias of 182% in the LZ (Fig. 8a) and a negative bias of 69–82% in the other basins (Fig. 8b–d) relative to the MODIS. This can be

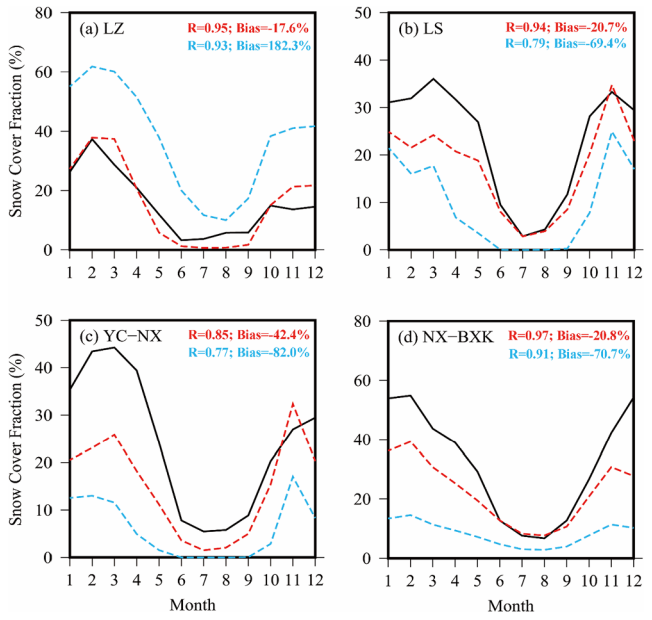

Fig. 8. Annual cycle of MODIS and VIC-Glacier simulated SCF (%) in the LZ, LS, YC-NX and NX-BXK sub-basins for 2001–2014.

explained by the large overestimates in the GLDAS precipitation in the LZ and underestimates in the original CMA data in other basins (Fig. 4). The apparent improvements of SCF simulations with the reconstructed precipitation demonstrate an improvement of precipitation input in hydrological modelling in the UB.

5. Comparison of reconstructed precipitation with other datasets

Evaluation studies have highlighted the striking differences in precipitation estimates from different data sources (e.g., the gauge-based, satellite-based, and reanalysis data, etc.) in the TP basins (Yin et al., 2008; Wang and Zeng, 2012; Gao and Liu, 2013; Tong et al., 2014b; You et al., 2015). Table 4 compares the mean annual precipitation of reconstructed data with the widely used precipitation datasets in the UB basins, including the gauge-based APHRODITE, satellite-based PERSIANN-CDR and GPM, reanalysis data of GLDAS and ERA-Interim, and the outputs of the regional climate model HAR.

Considerable disagreement is observed among the precipitation estimates, with mean annual precipitation average in the UB ranging from 500 mm in the APHRODITE to 1465 mm in the ERA-Interim (Table 4). The widely used gauge-based APHRODITE tends to underestimate the reconstructed precipitation (22–43%) in all the sub-basins, resulting in a mean negative bias of 32% (Table 4). The GPM and HAR tend to underestimate the reconstructed precipitation in most of the sub-basins (except for the LZ and NX-BXK), with the largest underestimates seen in the LS and YC-NX (24–50%). On the other hand, the reanalysis data ERA-Interim and infrared-based PERSIANN-CDR largely overestimate the reconstructed precipitation, with the largest bias of 127–162% in the ERA-Interim (Table 4). No consistent pattern is presented in the GLDAS, with four basins having a positive bias of 62–113% and three with negative bias of 11–38%, resulting in a mean positive bias of 11% in the UB (Table 4).

The large variety of mean annual precipitation estimates in Table 4 suggests that high mountain precipitation is still not well represented in either satellite-based precipitation, reanalysis or regional climate models. Given the large number of gauges involved and the validation through hydrological model simulations, the reconstructed precipitation in this study best represent the real precipitation amount thus far in the UB basin.

6. Discussion

6.1. Impact of precipitation input on estimates of meltwater contribution

Glacier and snow melt are important hydrological processes which can significantly modify streamflow regimes (Immerzeel et al., 2010; Zhang et al., 2013). However, the relative contribution of meltwater to runoff differs fundamentally under different precipitation estimates (Bookhagen and Burbank, 2010; Zhang et al., 2013; Su et al., 2016).

With the same VIC-Glacier model driven by gridded CMA data multiplied by a correction factor of 1.33, Zhang et al. (2013) estimated a contribution of 11.6% from glacier runoff to total flow at the Nuxia station (NX) for 1961–1999. This estimate is less than the contribution of 13.5% estimated from current work for the same period, although the mean annual precipitation averaged in the NX was nearly the same used in Zhang et al. (2013) (540 mm) and in this work (544 mm). A close inspection shows that large differences exist in sub-basins between mean annual precipitation estimates from Zhang et al. (2013) and the current study (Table S3), which may explain the discrepancy in glacier runoff contribution from the two studies.

Chen et al. (2017) and Zhao et al. (2019) also estimated glacier runoff contributions of 9.9% and 5.5% to total runoff of NX, respectively, with either different hydrological models or different precipitation correction approaches. However, the exact amount of precipitation input used in the studies was not clearly indicated at any time scales. Although other factors (e.g., temperature and models) also affect flow composition simulations, accurate precipitation inputs are still the prerequisite to acquire reasonable model parameters and reliable model results (Zhang et al., 2013).

To investigate how precipitation affects runoff components simulation, the NX-BXK sub-basin where glacier and snow melt account for about 45.3% and 15.1% of total runoff (Fig. 6), respectively, is selected for sensitivity analysis with the VIC-Glacier model (Fig. 9). The contribution from glacier runoff shows a decreasing trend with the increase of precipitation, while snowmelt and rainfall contributions tend to increase with precipitation, suggesting an overestimate/underestimate of precipitation being compensated by an underestimate/overestimate of glacier melt in the model simulation.

We observed that the contribution of glacier and rainfall runoff tend to have a larger sensitivity to precipitation decrease than to precipitation increase. For instance, the contribution of glacier runoff would increase about 7–10% with the unit decrease of mean annual precipitation, while it would decrease about 4–5% with the unit increase of precipitation (Fig. 9). Therefore, the widely recognized underestimates in current gridded precipitation datasets for high mountains (Immerzeel et al., 2015; Dahri et al., 2016; Kan et al., 2018) may result in large uncertainties in meltwater contribution calculations in glacier-affected basins.

6.2. Two correction approaches for high mountain precipitation

In this work, orographic correction approach is used in the RKZ, while linear correction in the other basins. There are total 10 rain gauges in the RKZ and there is a good correspondence in mean annual precipitation estimates between rain gauges and the corresponding CMA grids (Fig. 10a). We find that the linear correction approach is also suitable to the RKZ, which results in comparable precipitation (429 mm/yr) and streamflow estimates (NSE = 0.82, Bias = −2.1%) with the orographic correction approach (439 mm/yr) in the basin (Fig. 10b, c). However, linear correction approach highly relies on an acceptable station density. Fig. 10d shows that the linearly corrected mean annual precipitation would decrease from 429 mm to 409 mm when the number of rain gauges reduce from 10 to 4 in the basin.

The orographic correction approach has been widely used in deriving high mountain precipitation from low elevations (Alijani, 2008; Bookhagen and Burbank, 2006; Dahri et al., 2016; Kan et al., 2018). However Sun et al. (2020) demonstrate that precipitation gradients show

Table 4
Mean annual precipitation estimates from the reconstructed data and other data sources in the UB and its sub-basins.

	APHRODITE (1979–2007)	Reconstructed (1979–2007)	Bias (%)	HAR (2001–2013)	Reconstructed (2001–2013)	Bias (%)	GPM (2015–2016)	Reconstructed (2015–2016)	Bias (%)	PERSIANN-CDR (1983–2016)
LZ	254	370	−31	466	356	31	308	281	10	739
LZ-NGS	314	433	−28	545	446	22	258	348	−26	814
RKZ	328	435	−25	328	426	−23	331	392	−16	657
LS	504	649	−22	466	676	−31	414	613	−32	765
NGS-YC	360	488	−26	495	503	−1	284	485	−41	803
YC-NX	537	946	−43	719	945	−24	528	1060	−50	1025
NX-BXK	981	1418	−31	1430	1318	9	1011	961	5	883
UB	500	734	−32	645	717	−10	660	620	6	773

	Reconstructed (1983–2016)	Bias (%)	GLDAS (1961–2016)	Reconstructed (1961–2016)	Bias (%)	ERA-Interim (1979–2016)	Reconstructed (1979–2016)	Bias (%)
LZ	355	108	721	366	97	821	361	127
LZ-NGS	444	83	789	443	78	787	434	82
RKZ	436	51	937	439	113	1130	432	162
LS	652	17	566	637	−11	612	647	−5
NGS-YC	491	64	792	489	62	670	485	38
YC-NX	950	8	729	911	−20	2337	940	149
NX-BXK	1359	−35	828	1325	−38	2515	1367	84
UB	722	7	786	709	11	1465	720	103

Note: PERSIANN-CDR = Precipitation Estimation from Remotely Sensed Information using Artificial Neural Networks-Climate Data Record; GLDAS = Global Land Data Assimilation System; HAR = High Asia Refined analysis; GPM = Global Precipitation Measurement; APHRODITE = Asian Precipitation- Highly-Resolved Observational Data Integration Towards Evaluation of the Water Resources; CMA = China Meteorological Administration; ERA = reanalysis dataset produced by the European Center for Medium-Range Weather Forecasts.

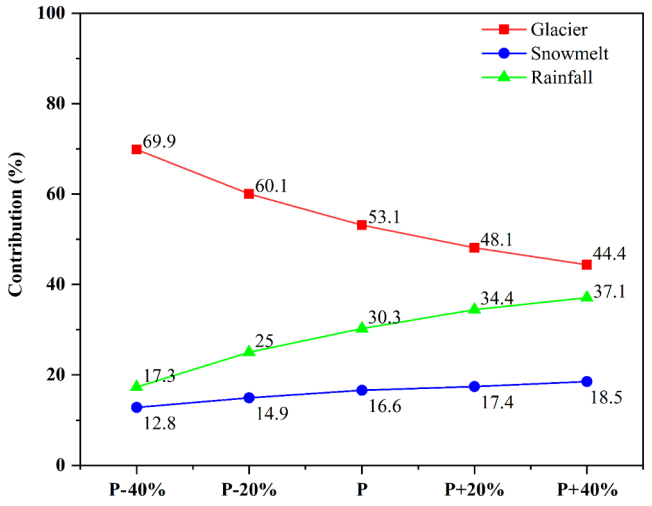

Fig. 9. Sensitivity of glacier, snowmelt and rainfall runoff contribution to the changes of precipitation for 1980–2000 in the NX-BXK sub-basin.

contrast characteristics between westerlies- and monsoon-dominated river basins in the TP. Precipitation enhancement due to orographic lifting is apparent in the westerly basins (i.e. upper Yarkant, upper Indus, upper Amu Darya, upper Syr Darya), while mean annual precipitation generally shows decreasing trends with elevation in the monsoon basins, i.e. upper Yangtze, upper Yellow, Lancang, Nujiang, upper Brahmaputra basins (Sun et al., 2020). The orographic effects on precipitation are only observed at relatively smaller scales in the monsoon basins, such as, the very source regions of the upper Lancang and Nujiang (Sun et al., 2020), consistent with the findings in this work. Therefore, basin size and climate control should be considered when using the orographic correction approach to derive high mountain precipitation from low elevations. Along with the progress of the Second Tibetan Plateau Scientific Expedition and Research, more meteorological observations will be established, which is expected to benefit reliable precipitation estimates and hydrological studies in the region.

7. Conclusion

In this work, a gridded daily precipitation dataset (10 km × 10 km) is reconstructed in the UB for 1961–2016, based on 262 rain gauges through combining orographic and linear corrections of CMA and GLDAS data, and the reconstructed precipitation is inversely evaluated by the VIC-Glacier hydrological model. The main results of the study are summarized as below:

1. The corrections greatly improved the precipitation estimates in the UB and the basin-averaged mean annual precipitation increased from 465 mm in the original data to 709 mm in the reconstructed

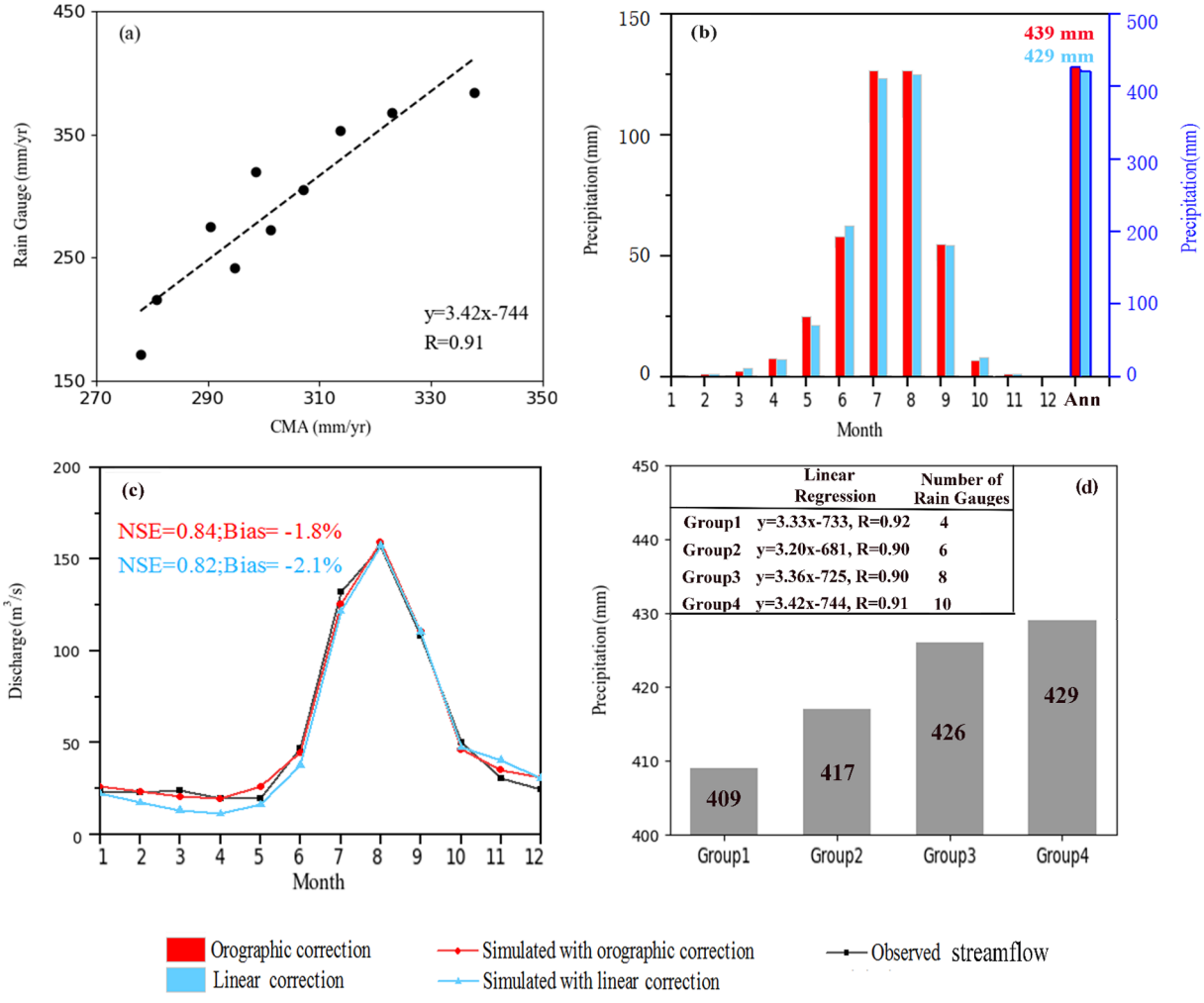

Fig. 10. Scatterplot of mean annual precipitation from rain gauges against the corresponding CMA gridded data for 2014–2016 (a), corrected precipitation with linear and orographic corrections (b), simulated streamflow with two corrected precipitation inputs (c), and corrected precipitation estimates with linear correction with different number of rain gauges (d) in the RKZ sub-basin.

data for 1961–2016. The inverse hydrological model evaluation demonstrates the accuracy and rationality of the reconstructed precipitation as input for hydrological modeling in the UB.
2. Large uncertainties exist in mean annual precipitation estimates in the UB with a range of 500–1465 mm among seven datasets. The reconstructed precipitation from this work involves a large number of rain gauges and extensive hydrological validation and may best represent the real precipitation amount thus far in the UB basin.
3. The monsoon-dominated UB basin exhibits an overall negative precipitation vertical gradient, with apparent orographic lifting only appearing at local scales or in small basins. Basin size and climate control should be considered when using the orographic correction approach to derive high mountain precipitation, and combining different correction approaches is recommended.

CRediT authorship contribution statement

He Sun: Conceptualization, Formal analysis, Investigation, Methodology, Resources, Visualization, Writing - original draft. **Fengge Su:** Conceptualization, Formal analysis, Investigation, Methodology, Resources, Visualization, Funding acquisition, Writing - review & editing.

Declaration of Competing Interest

The authors declare that they have no known competing financial interests or personal relationships that could have appeared to influence the work reported in this paper.

Acknowledgements

This work was financially supported by the National Natural Science Foundation of China (91747201, 41871057), the Second Tibetan Plateau Scientific Expedition and Research Program (2019 QZKK0201) and the “Strategic Priority Research Program” of the Chinese Academy of Sciences (XDA20060202).

Appendix A. Supplementary data

Supplementary data to this article can be found online at https://doi.org/10.1016/j.jhydrol.2020.125484.

References

Alijani, B., 2008. Effect of the Zagros Mountains on the spatial distribution of precipitation. J. Mt. Sci. 5 (3), 218–231. https://doi.org/10.1007/s11629-008-0126-8.
Ashouri, H., Hsu, K.-L., Sorooshian, S., et al., 2015. PERSIANN-CDR: Daily precipitation climate data record from multisatellite observations for hydrological and climate studies. Bull. Amer. Meteorol. Soc. 96 (1), 69–83. https://doi.org/10.1175/bams-d-13-00068.1.
Bahr, D.B., Meier, M.F., Peckham, S.D., 1997. The physical basis of glacier volume-area scaling. J. Geophys. Res. Solid Earth. 102 (B9), 20355–20362. https://doi.org/10.1029/97jb01696.
Bai, P., Liu, X., Yang, T., et al., 2016. Evaluation of streamflow simulation results of land surface models in GLDAS on the Tibetan plateau. J. Geophys. Res. Atmos. 121 (20), 12180–12197. https://doi.org/10.1002/2016jd025501.
Bookhagen, B., Burbank, D.W., 2006. Topography, relief, and TRMM-derived rainfall variations along the Himalaya. Geophys. Res. Lett. 33 (8). https://doi.org/10.1029/2006gl026037.
Bookhagen, B., Burbank, D.W., 2010. Toward a complete Himalayan hydrological budget: Spatiotemporal distribution of snowmelt and rainfall and their impact on river discharge. J. Geophys. Res. 115 (F3). https://doi.org/10.1029/2009jf001426.
Chen, A., Chen, D., Azorin-Molina, C., 2018a. Assessing reliability of precipitation data over the Mekong River Basin: A comparison of ground-based, satellite, and reanalysis datasets. Int. J. Climatol. 38 (11), 4314–4334. https://doi.org/10.1002/joc.5670.
Chen, X., Long, D., Hong, Y., et al., 2018b. Climatology of snow phenology over the Tibetan plateau for the period 2001–2014 using multisource data. Int. J. Climatol. 38 (6), 2718–2729. https://doi.org/10.1002/joc.5455.
Chen, X., Long, D., Hong, Y., et al., 2017. Improved modeling of snow and glacier melting by a progressive two-stage calibration strategy with GRACE and multisource data: How snow and glacier meltwater contributes to the runoff of the Upper Brahmaputra River basin? Water Resour. Res. 53, 2431–2466. https://doi.org/10.1002/2016WR019656.
Cuo, L., Zhang, Y., Bohn, T.J., et al., 2015. Frozen soil degradation and its effects on surface hydrology in the northern Tibetan Plateau. J. Geophys. Res. Atmos. 120 (16), 8276–8298. https://doi.org/10.1002/2015jd023193.
Curio, J., Maussion, F., Scherer, D., 2015. A 12-year high-resolution climatology of atmospheric water transport over the Tibetan Plateau. Earth Syst. Dynam. 6 (1), 109–124. https://doi.org/10.5194/esd-6-109-2015.
Dahri, Z.H., Ludwig, F., Moors, E., et al., 2016. An appraisal of precipitation distribution in the high-altitude catchments of the Indus basin. Sci. Total Environ. 548–549, 289–306. https://doi.org/10.1016/j.scitotenv.2016.01.001.
Duethmann, D., Zimmer, J., Gafurov, A., et al., 2013. Evaluation of areal precipitation estimates based on downscaled reanalysis and station data by hydrological modelling. Hydrol. Earth Syst. Sci. 17 (7), 2415–2434. https://doi.org/10.5194/hess-17-2415-2013.
Gao, Y., Liu, M., 2013. Evaluation of high-resolution satellite precipitation products using rain gauge observations over the Tibetan Plateau. Hydrol. Earth Syst. Sci. 17 (2), 837–849. https://doi.org/10.5194/hess-17-837-2013.
Guan, Z., Chen, C., Ou, Y., 1984. The Rivers and the Lakes in Tibet. Science and Technology Press, Beijing.
Guo, D., Wang, H., Li, D., 2012. A projection of permafrost degradation on the Tibetan Plateau during the 21st century. J. Geophys. Res. Atmos. 117 (D5), n/a-n/a. https://doi.org/10.1029/2011jd016545.
D.K. Hall G.A. Riggs V.V. Salomonson et al. MODIS snow-cover products Remote Sens. Environ. 83 1–2 2002 181 194 https://doi.org/PiiS0034-4257(02)00095-0.
He, J., Yang, K., 2011. China meteorological forcing dataset. Cold Arid Regions Sci. Data Center at Lanzhou. https://doi.org/10.3972/westdc.002.2014.db.
Hock, R., 2003. Temperature index melt modelling in mountain areas. J. Hydrol. 282 (1–4), 104–115. https://doi.org/10.1016/s0022-1694(03)00257-9.
Huang, X., Wang, Z., Sang, Y., et al., 2016. Precision of data in three precipitation datasets of the Yarlung Zangbo River Basin. Progr. Geogr. 35 (3), 339–348.
Huffman, G.J., Bolvin, D.T., Braithwaite, D. et al., 2014. Algorithm Theoretical Basis Document (ATBD) Version 4.4 for the NASA Global Precipitation Measurement (GPM) Integrated Multi-satellitE Retrievals for GPM (I-MERG). GPM Project, Greenbelt, MD,, 30 PP. http://pmm.nasa.gov/sites/default/files/document_files/IMERG_ATBD_V4.4.pdf .
Huffman, G.J., Bolvin, D.T., Braithwaite, D., et al., 2015. NASA global precipitation measurement (GPM) integrated multi-satellite retrievals for GPM (IMERG). Algorithm Theoretical Basis Document, version. 4, 30.
Huffman, G.J., Bolvin, D.T., Nelkin, E.J., et al., 2007. The TRMM multisatellite precipitation analysis (TMPA): Quasi-global, multiyear, combined-sensor precipitation estimates at fine scales. J. Hydrometeorol. 8 (1), 38–55. https://doi.org/10.1175/jhm560.1.
Immerzeel, W.W., van Beek, L.P., Bierkens, M.F., 2010. Climate change will affect the Asian water towers. Science 328 (5984), 1382–1385. https://doi.org/10.1126/science.1183188.
Immerzeel, W.W., Wanders, N., Lutz, A.F., et al., 2015. Reconciling high-altitude precipitation in the upper Indus basin with glacier mass balances and runoff. Hydrol. Earth Syst. Sci. 19 (11), 4673–4687. https://doi.org/10.5194/hess-19-4673-2015.
Jiang, S., Ren, L., Hong, Y., et al., 2012. Comprehensive evaluation of multi-satellite precipitation products with a dense rain gauge network and optimally merging their simulated hydrological flows using the Bayesian model averaging method. J. Hydrol. 452–453, 213–225. https://doi.org/10.1016/j.jhydrol.2012.05.055.
Joyce, R.J., Janowiak, J.E., Arkin, P.A., et al., 2004. CMORPH: A method that produces global precipitation estimates from passive microwave and infrared data at high spatial and temporal resolution. J. Hydrometeorol. 5 (3), 487–503. https://doi.org/10.1175/1525-7541(2004)005<0487:Camtpg>2.0.Co;2.
Kan, B., Su, F., Xu, B., et al., 2018. Generation of high mountain precipitation and temperature data for a quantitative assessment of flow regime in the upper yarkant basin in the karakoram. J. Geophys. Res. Atmos. 123 (16), 8462–8486. https://doi.org/10.1029/2017jd028055.
R.B. Kayastha Study of glacier ablation in the Nepalese Himalayas by the energy balance model and positive degree-day method PhD Thesis 2001 Nagoya University 95 pp.
Khandu, Awange, J.L., Kuhn, M., et al., 2017. Changes and variability of precipitation and temperature in the Ganges-Brahmaputra-Meghna River Basin based on global high-resolution reanalyses. Int. J. Climatol. 37 (4), 2141–2159. https://doi.org/10.1002/joc.4842.
Kuang, X., Jiao, J., 2016. Review on climate change on the Tibetan Plateau during the last half century. J. Geophys. Res. Atmos. 121 (8), 3979–4007. https://doi.org/10.1002/2015jd024728.
Kumar, R., Singh, S., Kumar, R., et al., 2016. Development of a glacio-hydrological model for discharge and mass balance reconstruction. Water Resour. Manag. 30 (10), 3475–3492. https://doi.org/10.1007/s11269-016-1364-0.
Li, B., Zhou, W., Zhao, Y., et al., 2015. Using the SPEI to assess recent climate change in the yarlung zangbo river basin. South Tibet. Water 7 (10), 5474–5486. https://doi.org/10.3390/w7105474.
Li, C., Su, F., Yang, D., et al., 2018. Spatiotemporal variation of snow cover over the Tibetan Plateau based on MODIS snow product, 2001–2014. Int. J. Climatol. 38 (2), 708–728. https://doi.org/10.1002/joc.5204.
Li, F., Xu, Z., Feng, Y., et al., 2012. Changes of land cover in the Yarlung Tsangpo River basin from 1985 to 2005. Environ. Earth Sci. 68 (1), 181–188. https://doi.org/10.1007/s12665-012-1730-z.
Li, F., Zhang, Y., Xu, Z., et al., 2013. The impact of climate change on runoff in the southeastern Tibetan Plateau. J. Hydrol. 505, 188–201. https://doi.org/10.1016/j.jhydrol.2013.09.052.
Liang, X., Lettenmaie, D.P., Wood, E.F., et al., 1994. A simple hydrologically based model of land-surface water and energy fluxes. J. Geophys. Res. Atmos. 99:(D7), 14415–14428. https://doi.org/10.1029/94jd00483.
Liang, X., Lettenmaier, D.P., Wood, E.F., 1996. One-dimensional statistical dynamic

representation of subgrid spatial variability of precipitation in the two-layer variable infiltration capacity model. J. Geophys. Res. Atmos. 101 (D16), 21403–21422. https://doi.org/10.1029/96jd01448.
Liu, J., Xu, Z., Bai, J., et al., 2018. Assessment and correction of the PERSIANN-CDR Product in the Yarlung Zangbo River Basin. China. Remote Sens. 10 (12), 2031. https://doi.org/10.3390/rs10122031.
Liu, J., Zhang, W., 2018. Spatial variability in degree-day factors in yarlung zangbo river basin in china. J. Univ. Chin. Acad. Sci. https://doi.org/10.7523/j.issn.2095-6134.2018.05.018.
Liu, R., Ma, Y., Yang, Y., et al., 2017a. Error analysis of ensemble multi-satellite precipitation datasets over the tibetan plateau. Int. Geosci. Remote Se. 4684–4687. https://doi.org/10.1109/igarss.2017.8128047.
Liu, X., Yang, T., Hsu, K.L., et al., 2017b. Evaluating the streamflow simulation capability of PERSIANN-CDR daily rainfall products in two river basins on the Tibetan Plateau. Hydrol. Earth Syst. Sci. 21 (1), 169–181. https://doi.org/10.5194/hess-21-169-2017.
Liu, Z., Tian, L., Yao, T., et al., 2007. Temporal and spatial variations of δ18O in precipitation of the Yarlung Zangbo River Basin. J. Geogr. Sci. 17 (3), 317–326. https://doi.org/10.1007/s11442-007-0317-1.
Lu, D., Yong, B., 2018. Evaluation and Hydrological Utility of the Latest GPM IMERG V5 and GSMaP V7 Precipitation Products over the Tibetan Plateau. Remote Sens. 10 (12), 2022. https://doi.org/10.3390/rs10122022.
Lutz, A.F., Immerzeel, W.W., Shrestha, A.B., et al., 2014. Consistent increase in High Asia's runoff due to increasing glacier melt and precipitation. Nat. Clim. Chang. 4 (7), 587–592. https://doi.org/10.1038/nclimate2237.
Ma, Y., Hong, Y., Chen, Y., et al., 2018. Performance of optimally merged multisatellite precipitation products using the dynamic bayesian model averaging scheme over the tibetan plateau. J. Geophys. Res. Atmos. 123 (2), 814–834. https://doi.org/10.1002/2017jd026648.
Ma, Y., Tang, G., Long, D., et al., 2016. Similarity and error intercomparison of the GPM and its predecessor-TRMM multisatellite precipitation analysis using the best available hourly gauge network over the tibetan plateau. Remote Sens. 8 (7), 569. https://doi.org/10.3390/rs8070569.
Ma, Y., Zhang, Y., Yang, D., et al., 2015. Precipitation bias variabilityversusvarious gauges under different climatic conditions over the Third Pole Environment (TPE) region. Int. J. Climatol. 35 (7), 1201–1211. https://doi.org/10.1002/joc.4045.
Maussion, F., Scherer, D., Mölg, T., et al., 2014. Precipitation seasonality and variability over the tibetan plateau as resolved by the high asia reanalysis*. J. Clim. 27 (5), 1910–1927. https://doi.org/10.1175/jcli-d-13-00282.1.
Meng, F., Su, F., Li, Y., et al., 2019. Changes in terrestrial water storage during 2003–2014 and possible causes in tibetan plateau. J. Geophys. Res. Atmos. 124 (6), 2909–2931. https://doi.org/10.1029/2018jd029552.
Mimeau, L., Esteves, M., Jacobi, H.-W., et al., 2019. Evaluation of gridded and in-situ precipitation datasets on modeled glacio-hydrologic response of a small glacierized Himalayan catchment. J. Hydrometeorol. 20 (6), 1103–1121. https://doi.org/10.1175/jhm-d-18-0157.1.
Qi, W., Liu, J., Chen, D., 2018. Evaluations and improvements of GLDAS2.0 and GLDAS2.1 forcing data's applicability for basin scale hydrological simulations in the tibetan plateau. J. Geophys. Res. Atmos. 123 (23), 13128–13148. https://doi.org/10.1029/2018jd029116.
Rienecker, M.M., Suarez, M.J., Gelaro, R., et al., 2011. MERRA: NASA's modern-era retrospective analysis for research and applications. J. Clim. 24 (14), 3624–3648. https://doi.org/10.1175/Jcli-D-11-00015.1.
Rodell, M., Houser, P.R., Jambor, U., et al., 2004. The global land data assimilation system. Bull. Amer. Meteorol. Soc. 85 (3), 381–394. https://doi.org/10.1175/bams-85-3-381.
Simmons, A., Uppala, S., Dee, D.P., et al., 2006. ERA-interim: New ECMWF reanalysis products from 1989 onwards. ECMWF Newsletter. 110, 25–35.
Singh, P., Kumar, N., Arora, M., 2000. Degree–day factors for snow and ice for Dokriani Glacier, Garhwal Himalayas. J. Hydrol. 235(1-2), 1-11. https://doi.org/Doi 10.1016/S0022-1694(00)00249-3.
Sorooshian, S., AghaKouchak, A., Arkin, P., et al., 2011. Advancing the remote sensing of precipitation. Bull. Amer. Meteorol. Soc. 92 (10), 1271–1272. https://doi.org/10.1175/bams-d-11-00116.1.
Su, F., Adam, J.C., Bowling, L.C., et al., 2005. Streamflow simulations of the terrestrial Arctic domain. J. Geophys. Res. 110 (D8). https://doi.org/10.1029/2004jd005518.
Su, F., Gao, H., Huffman, G.J., et al., 2011. Potential utility of the real-time TMPA-RT precipitation estimates in streamflow prediction. J. Hydrometeorol. 12 (3), 444–455. https://doi.org/10.1175/2010jhm1353.1.
Su, F., Hong, Y., Lettenmaier, D.P., 2008. Evaluation of TRMM multisatellite precipitation analysis (TMPA) and its utility in hydrologic prediction in the la plata basin. J. Hydrometeorol. 9 (4), 622–640. https://doi.org/10.1175/2007jhm944.1.
Su, F., Zhang, L., Ou, T., et al., 2016. Hydrological response to future climate changes for the major upstream river basins in the Tibetan Plateau. Glob. Planet. Change. 136, 82–95. https://doi.org/10.1016/j.gloplacha.2015.10.012.
Sun, H., Su, F., Huang, J., et al., 2020. Contrasting precipitation gradient characteristics between westerlies and monsoon dominated upstream river basins in the Third Pole. Chin. Sci. Bull. 65 (1), 91–104. https://doi.org/10.1360/tb-2019-0491.
Tang, G., Behrangi, A., Long, D., et al., 2018. Accounting for spatiotemporal errors of gauges: A critical step to evaluate gridded precipitation products. J. Hydrol. 559, 294–306. https://doi.org/10.1016/j.jhydrol.2018.02.057.
Tong, K., Su, F., Xu, B., 2016. Quantifying the contribution of glacier meltwater in the expansion of the largest lake in Tibet. J. Geophys. Res. Atmos. 121 (19), 11158–11173. https://doi.org/10.1002/2016jd025424.
Tong, K., Su, F., Yang, D., et al., 2014a. Evaluation of satellite precipitation retrievals and their potential utilities in hydrologic modeling over the Tibetan Plateau. J. Hydrol. 519, 423–437. https://doi.org/10.1016/j.jhydrol.2014.07.044.
Tong, K., Su, F., Yang, D., et al., 2014b. Tibetan Plateau precipitation as depicted by gauge observations, reanalyses and satellite retrievals. Int. J. Climatol. 34 (2), 265–285. https://doi.org/10.1002/joc.3682.
Uppala, S.M., Kållberg, P., Simmons, A., et al., 2005. The ERA-40 re-analysis. Q. J. R. Meteorol. Soc. 131 (612), 2961–3012. https://doi.org/10.1256/qj.04.176.
Wang, A., Zeng, X., 2012. Evaluation of multireanalysis products with in situ observations over the Tibetan Plateau. J. Geophys. Res. Atmos. 117 (D5). https://doi.org/10.1029/2011jd016553.
Wang, L., Sun, L., Shrestha, M., et al., 2016. Improving snow process modeling with satellite-based estimation of near-surface-air-temperature lapse rate. J. J. Geophys. Res. Atmos. 121 (20), 12005–12030. https://doi.org/10.1002/2016jd025506.
Wang, L., Zhang, F., Zhang, H., et al., 2018a. Intensive precipitation observation greatly improves hydrological modelling of the poorly gauged high mountain Mabengnong catchment in the Tibetan Plateau. J. Hydrol. 556, 500–509. https://doi.org/10.1016/j.jhydrol.2017.11.039.
Wang, X., Pang, G., Yang, M., 2018b. Precipitation over the Tibetan Plateau during recent decades: a review based on observations and simulations. Int. J. Climatol. 38 (3), 1116–1131. https://doi.org/10.1002/joc.5246.
Wang, X., Pang, G., Yang, M., et al., 2017. Evaluation of climate on the Tibetan Plateau using ERA-Interim reanalysis and gridded observations during the period 1979–2012. Quat. Int. 444, 76–86. https://doi.org/10.1016/j.quaint.2016.12.041.
Wortmann, M., Bolch, T., Menz, C., et al., 2018. Comparison and correction of high-mountain precipitation data based on glacio-hydrological modeling in the tarim river Headwaters (High Asia). J. Hydrometeorol. 19 (5), 777–801. https://doi.org/10.1175/jhm-d-17-0106.1.
Wu, Q., Kang, S., Gao, T., et al., 2010. The characteristics of the positive degree-day factors of the Zhadang glacier on the Nyainqentanglha range of Tibetan Plateau, and its application. J. Glaciol. Geocryol. 32 (5), 891–897.
Wu, Q., Zhang, T., 2010. Changes in active layer thickness over the Qinghai-Tibetan Plateau from 1995 to 2007. J. Geophys. Res. Atmos. 115 (D9). https://doi.org/10.1029/2009JD012974.
Yang, D., Kane, D., Zhang, Z., et al., 2005. Bias corrections of long-term (1973–2004) daily precipitation data over the northern regions. Geophys. Res. Lett. 32 (19). https://doi.org/10.1029/2005gl024057.
Yang, W., Guo, X., Yao, T., et al., 2011. Summertime surface energy budget and ablation modeling in the ablation zone of a maritime Tibetan glacier. J. Geophys. Res. Atmos. 116 (D14). https://doi.org/10.1029/2010jd015183.
Yang, Y., Gao, D., Li, B., 1989. Study on the moisture passage on the lower reaches of the Yarlung Zangbo river. Sci. China (Series B) 32 (5), 580–593. https://doi.org/10.1351/pac198961050973.
Yang, Z., Zhuo, M., Lu, H. et al., 2014. Characteristics of precipitation variation and its effects on runoff in the Yarlung Zangbo River basin during 1961–2010. Journal of Glaciology and Geocryology. 36(1), 166-72. https://doi.org/10.7522 /j.issn.1000-0240.2014.0021.
Yao, T., 2004. Recent glacial retreat in High Asia in China and its impact on water resource in Northwest China. Sci. China (Series D). 47 (12), 1065. https://doi.org/10.1360/03yd0256.
Yao, T., Thompson, L., Yang, W., et al., 2012. Different glacier status with atmospheric circulations in Tibetan Plateau and surroundings. Nat. Clim. Chang. 2 (9), 663–667. https://doi.org/10.1038/nclimate1580.
Yatagai, Kamiguchi, K., Arakawa, O., et al., 2012. APHRODITE: Constructing a long-term daily gridded precipitation dataset for asia based on a dense network of rain gauges. Bull. Amer. Meteorol. Soc. 93 (9), 1401–1415. https://doi.org/10.1175/bams-d-11-00122.1.
Ye, Q., Zong, J., Tian, L., et al., 2017. Glacier changes on the Tibetan Plateau derived from Landsat imagery: mid-1970s – 2000–13. J. Glaciol. 63 (238), 273–287. https://doi.org/10.1017/jog.2016.137.
Yin, Z.-Y., Zhang, X., Liu, X., et al., 2008. An assessment of the biases of satellite rainfall estimates over the tibetan plateau and correction methods based on topographic analysis. J. Hydrometeorol. 9 (3), 301–326. https://doi.org/10.1175/2007jhm903.1.
You, Q., Kang, S., Wu, Y., et al., 2007. Climate change over the Yarlung Zangbo River Basin during 1961–2005. J. Geogr. Sci. 17 (4), 409–420. https://doi.org/10.1007/s11442-007-0409-y.
You, Q., Min, J., Zhang, W., et al., 2015. Comparison of multiple datasets with gridded precipitation observations over the Tibetan Plateau. Clim. Dyn. 45 (3–4), 791–806. https://doi.org/10.1007/s00382-014-2310-6.
Zhang, L., Su, F., Yang, D., et al., 2013. Discharge regime and simulation for the upstream of major rivers over Tibetan Plateau. J. Geophys. Res. Atmos. 118 (15), 8500–8518. https://doi.org/10.1002/jgrd.50665.
Zhang, W., Zhang, L., Zhou, T., 2016. Interannual variability and the underlying mechanism of summer precipitation over the Yarlung Zangbo River basin. Chin. J. Atmos. Sci. 40 (5), 965–980.
Zhang, Y., Liu, S., Ding, Y., 2006. Observed degree-day factors and their spatial variation on glaciers in western China. Ann. Glaciol. 43, 301–306. https://doi.org/10.3189/172756406781811952.
Zhao, Q., Ding, Y., Wang, J., et al., 2019. Projecting climate change impacts on hydrological processes on the Tibetan Plateau with model calibration against the Glacier Inventory Data and observed streamflow. J. Hydrol. 573, 60–81. https://doi.org/10.1016/j.jhydrol.2019.03.043.
Zhou, J., Wang, L., Zhang, Y. et al., 2014. Exploring the water storage changes in the largest lake (Selin Co) over the Tibetan Plateau during 2003–2012 from a basin-wide hydrological modeling. Water Resour. Res. https://doi.org/10.1002/.